Monitoring the contact stress distribution of gecko-inspired adhesives using mechano-sensitive surface coatings

Jens W. Neubauer, Longjian Xue, Johann Erath, Dirk-M. Drotlef, Aránzazu del Campo, and Andreas Fery

ACS Appl. Mater. Interfaces, 2016, 8 (28), pp 17870–17877
DOI: 10.1021/acsami.6b05327

Keywords: adhesion; bioinspired; biomimetic; mechano-responsive; polyelectrolyte brushes; polymer brushess

Monitoring the Contact Stress Distribution of Gecko-Inspired Adhesives using Mechano-Sensitive Surface Coatings

Jens W. Neubauer,[†,§] *Longjian Xue,*[‡,#] *Johann Erath,*[§] *Dirk-M. Drotlef,*[#] *Aránzazu del Campo,**[||,□,#] *Andreas Fery**[†,▽,§]

[†] Leibniz-Institut für Polymerforschung Dresden e.V., Hohe Str. 6, 01069 Dresden, Germany

[‡] School of Power and Mechanical Engineering, Wuhan University, South Donghu Road 8, 430072 Wuhan, China

[§] Department of Physical Chemistry II, University of Bayreuth, Universitätsstr. 30, 95447 Bayreuth, Germany

[#] Max Planck Institute for Polymer Research, Ackermannweg 10, 55128 Mainz, Germany

[||] INM – Leibniz Institute for New Materials, Campus D2 2, 66123 Saarbrücken, Germany

[□] Chemistry Faculty, Saarland University, Campus D2 2, 66123 Saarbrücken, Germany

[▽] Chair of Physical Chemistry of Polymeric Materials, Technische Universität Dresden, Hohe Str. 6, 01069 Dresden, Germany

KEYWORDS bioinspired, biomimetic, adhesion, mechano-responsive, polymer brushes, polyelectrolyte brushes

ABSTRACT

The contact geometry of microstructured adhesive surfaces is of high relevance for adhesion enhancement. Theoretical considerations indicate that the stress distribution in the contact zone is crucial for the detachment mechanism, but direct experimental evidence is missing so far. In this work, we propose a method that allows, for the first time, the detection of local stresses at the contact area of biomimetic adhesive microstructures during contact formation, compression and detachment. We use a mechano-sensitive polymeric layer, which turns mechanical stresses into changes of fluorescence intensity. The biomimetic surface is brought into contact with this layer in a well-defined fashion using a micro-contact printer, while the contact area is monitored with fluorescence microscopy *in situ.* Thus, changes in stress distribution across the contact area during compression and pull-off can be visualized with a lateral resolution of 1 µm. We apply this method to study the enhanced adhesive performance of T-shaped micropillars, compared to flat punch microstructures. We find significant differences in the stress distribution of the both differing contact geometries during pull-off. In particular, we find direct evidence for the suppression of crack nucleation at the edge of T-shaped pillars, which confirms theoretical models for the superior adhesive properties of these structures.

INTRODUCTION

Animals have evolved hierarchical structures to adhere on different kinds of smooth and rough surfaces.[1,2] Inspired by this performance, various artificial structures have been fabricated.[3-13] In recent years, generic mechanisms of these structures have been identified.

One important mechanism is the so-called contact splitting:[1,14] Rather than exhibiting a continuous adhesion area, the biological and biomimetic systems mentioned above typically show a large number of isolated contact zones. Thus, the contact can be adapted to the surface roughness. Further, the crack propagation is limited and, in order to fully detach, a crack must be nucleated at each individual contact zone.

Besides contact splitting, another essential feature for outstanding adhesion performance is the contact geometry of the contact zones. Different contact geometries exist in biological models, adapted to their environment and distinguished between dry adhesion[15] and wet adhesion.[16-19] Familiar examples for dry adhesion are fibrils terminated with a spatula-shaped geometry on gecko feet pads,[20,21] or with a thin annular plate on beetle feet and plants (T-shaped geometry).[22]

With lithography methods, fibrillar and pillar-based structures mimicking these geometries can be achieved.[23-28] Especially T-shaped pillars significantly outperform flat punches in adhesion.[24,29,30] For T-shaped pillars, overhangs are generated centrosymmetrically at the top of flat punch pillars, see Figure 1.

To attain insight into their superior adhesion performance, the detachment mechanism of T-shaped pillars was investigated explicitly using different methods. Hossfeld *et al.*[30] performed peel-off experiments under varying angles. By optical tracking of the detachment, they could locate the crack nucleation, leading to detachment, at the center of the contact area. In conformity with their observations, finite element analysis predicted stress peaks at the same positions and low stress at the edges.

Varenberg and Gorb *et al.* utilized high-speed video recording to follow the nucleation and the propagation of cracks during pull-off normal to the contact area in air[31,32] and underwater.[33] They also located the crack nucleation at the center of the contact area of T-shapes propagating towards the edges. For flat punch micropillars, the cracks propagated from the edges to the center. Additionally, the resulting detachment was faster for flat punches. Further, they observed the same detachment mechanism for T-shapes underwater although the pull-off force was lower.

Paretkar *et al.* used *in situ* scanning electron microscopy to take a more global view on the detachment of flat punch and T-shaped pillars.[34] They attributed the advantage in adhesion to the stochastic effect of more T-shaped pillars than flat punches remaining attached at the same elongation during retraction so that the study shows the macroscopic effect of the different detachment mechanisms. Despite detailed investigation of the detachment mechanism, a direct measurement of the contact stresses during detachment has been missing so far.

In theoretical approaches, the stress distribution at the contact area of flat punch and T-shaped pillars was investigated in numerous studies.[35-42] For flat punch micropillars, stress singularities at the edges were predicted. In contrast, the stress distribution of T-shaped pillars was predicted to be minimal at the edges and tension to be concentrated at the center. These differences in the stress distributions are expected to be the cause of the respective detachment mechanisms, but have not been determined experimentally yet.

In this study, we link the already gained experimental observations of the detachment to the predictions made by theory. We use mechano-sensitive surfaces[43,44] to determine the contact stress distributions of biomimetic micropillar structures with flat punch and T-shape geometry. We have recently introduced a novel type of mechano-sensitive polymeric layer for resolving local stresses on the micrometer scale.[43] This mechano-sensitive surface coating is generated in a surface-initiated polymerization, resulting in a polyelectrolyte brush structure. It is labeled with a fluorescent dye that can be quenched by the polyelectrolyte brush. With the soft colloidal probe technique,[45] it could be demonstrated that the fluorescence of the polyelectrolyte brush is sensitive to mechanical triggers. Compressive and tensile stress can be distinguished with high spatial resolution (1 µm) in the optical fluorescence read-out (Figure 2). This unique approach allowed us to map the local stresses under micropillars during detachment.

RESULTS AND DISCUSSION

We prepared arrays of flat punch and T-shaped micropillars according to the approach published in our earlier work.[24,29] The preparation process is shown schematically in Figure 1. These arrays were integrated into a micro-contact printing system to control the contact formation with the mechano-sensitive surfaces. For this purpose, featureless flat micro-printing stamps were fabricated in custom-made micro-contact printing stamp blanks using featureless silicon masters in the molding stations. Then, polydimethylsiloxane (PDMS) was injected into the stamp cavity. After curing, the stamp was demolded from the cavity constricting parts. With a small amount of PDMS, either flat punch or T-shaped micropillar structures were connected to the micro-contact printing stamps in a final curing step.

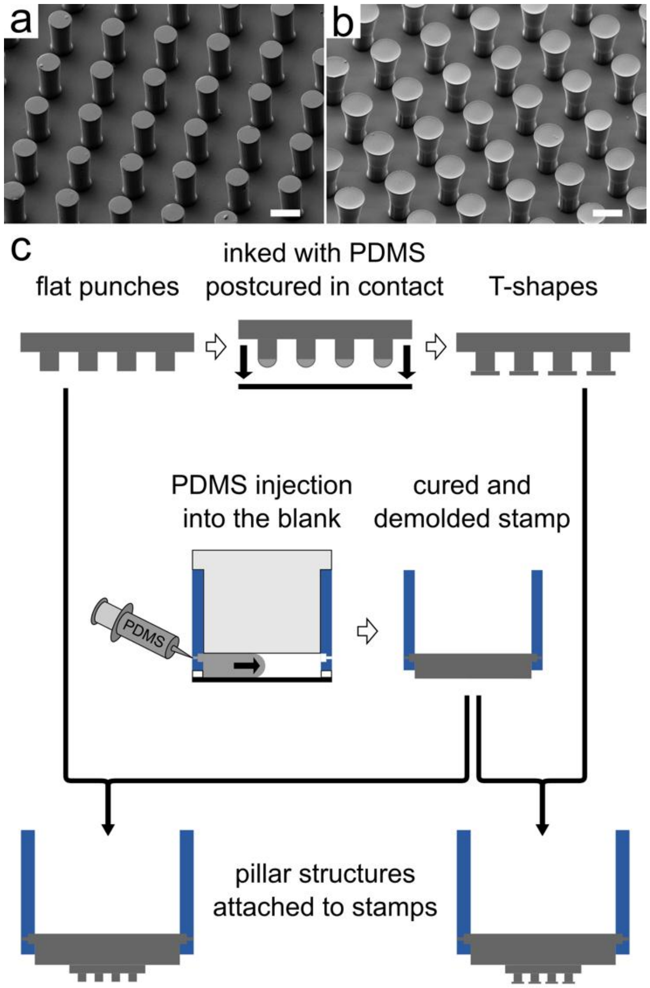

Figure 1. a) SEM micrograph of flat punch micropillars. **b)** SEM micrograph of T-shaped micropillars. The scale bars represent~~s~~ 20 µm for both micrographs. **c)** Fabrication scheme of the micro-contact printing stamps. The flat punch micropillar patterns were produced in a double soft molding procedure. Optionally, the flat punches were inked in a thin film of precured PDMS and postcured in contact to create T-shaped pillars. For featureless flat micro-contact printing stamps, PDMS was casted into the blue custom-made stamp blanks, using an unpatterned silicon master. After curing and demolding, flat punch or T-shaped pillar structures were attached to the stamp.

To determine stress distributions with resolution at the micrometer scale, we used a mechano-responsive polyelectrolyte brush.[43] This mechano-sensitive coating was polymerized from the surface and labeled with a fluorescent dye (carboxyfluorescein). In a previous article, we demonstrated its responsiveness to compressive and tensile stress.[43,45] Schematically, the mechanism is shown in Figure 2a.

Owing to solvent interactions, the equilibrium conformation of the polyelectrolyte brush is predominantly stretched, normal to the surface in aqueous media. The brush thickness was determined with atomic force microscopy force-distance measurements to be on the order of 150 nm.[46] As the dye can be quenched by the charges of the polyelectrolyte, most of the dye molecules are fluorescing in equilibrium. Compression leads to an increase in quenching, resulting in lower fluorescence intensity. On the contrary, tension further stretches the chains and decreases the quenching, generating a higher fluorescence intensity.[43] Accordingly, compressive and tensile stresses can be distinguished from the local fluorescence intensity and read-out optically with the high spatial resolution of confocal laser scanning microscopy (CLSM).

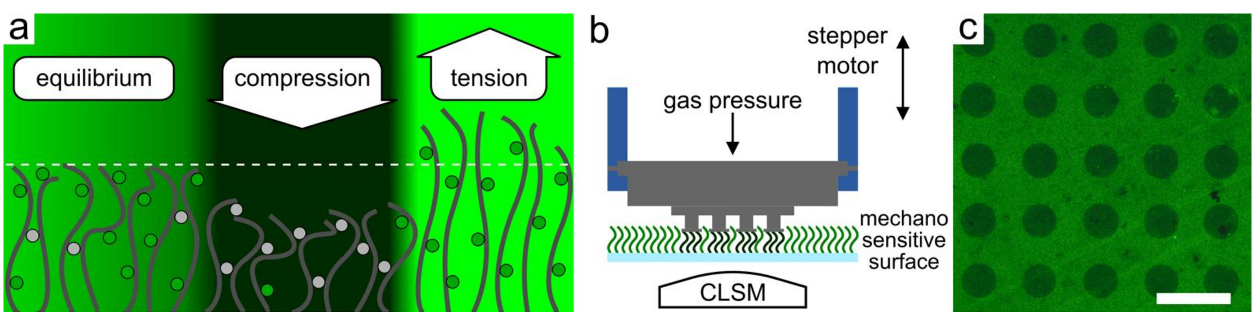

Figure 2. a) Scheme of the polyelectrolyte brush response mechanism to mechanical triggers. In water, the equilibrium conformation of the polyelectrolyte brush is predominantly stretched normal to the surface. Here, most of the dye molecules attached to the polyelectrolyte brush are fluorescing

(green dots). Quenching of the dye molecules can occur by cationic complexation in the polyelectrolyte chains (light grey dots). The compression of the structure decreases fluorescence, as most dye molecules are quenched. On the contrary, further stretching of the chains owing to external tension reduces quenching. **b)** Schematic alignment of the micro-contact printing stamps and the mechano-responsive surface on a confocal laser scanning microscope (CLSM). An overpressure can be applied in the stamp to bulge and compensate concavity. Moved by a stepper motor, the micropillars on the stamp are brought in contact with the mechano-sensitive surface. The pillars compress the brush structure so that the resulting quenching can be locally resolved with the CLSM. **c)** CLSM image of the mechano-sensitive polymer surface locally quenched by the approached T-shaped pillars. The scale bar depicts 50 µm.

We combined the micro-contact printing setup with a confocal laser scanning microscope to monitor the fluorescence response of the mechano-sensitive surface during approach and retraction of the microstructures (Figures 2b and S1). Thus, we were able to spatially resolve the fluorescence and deduce the local stresses during contact and detachment.

Prior to the approach, the micro-contact printing stamps with the structures were bulged with gas pressure to compensate their slightly concave shape that is due to shrinkage after curing. To avoid air entrapments while moving downwards,[47] the stamps were immersed carefully in the water that was wetting the polyelectrolyte brush. The polyelectrolyte brush is only responsive in aqueous media because it is collapsed in dried state and in non-solvents. After equilibrating, the stamp was further moved towards the surface with the stepper motor. Upon contact with the surface, dark spots of the size of the pillars could be observed in the CLSM (Figure 2c). The dark areas indicated quenching of the fluorescence as a consequence of the local compressive stress on the pillars.

In a typical experiment, the micropillars were moved against the mechano-sensitive surface with the stepper motor and retracted. CLSM images were taken in between the motor steps (Video S2).

For a detailed understanding of the detachment mechanism of the micropillars, images of individual pillars were taken into closer investigation. On a flat punch pillar, the fluorescence response at different steps during approach and retraction was investigated by azimuthally averaging the fluorescence intensity in the contact area (Figure 3). For comparison, the fluorescence intensity was normalized to the equilibrium intensity of the mechano-sensitive surface outside of the contact area, which served as an internal reference.

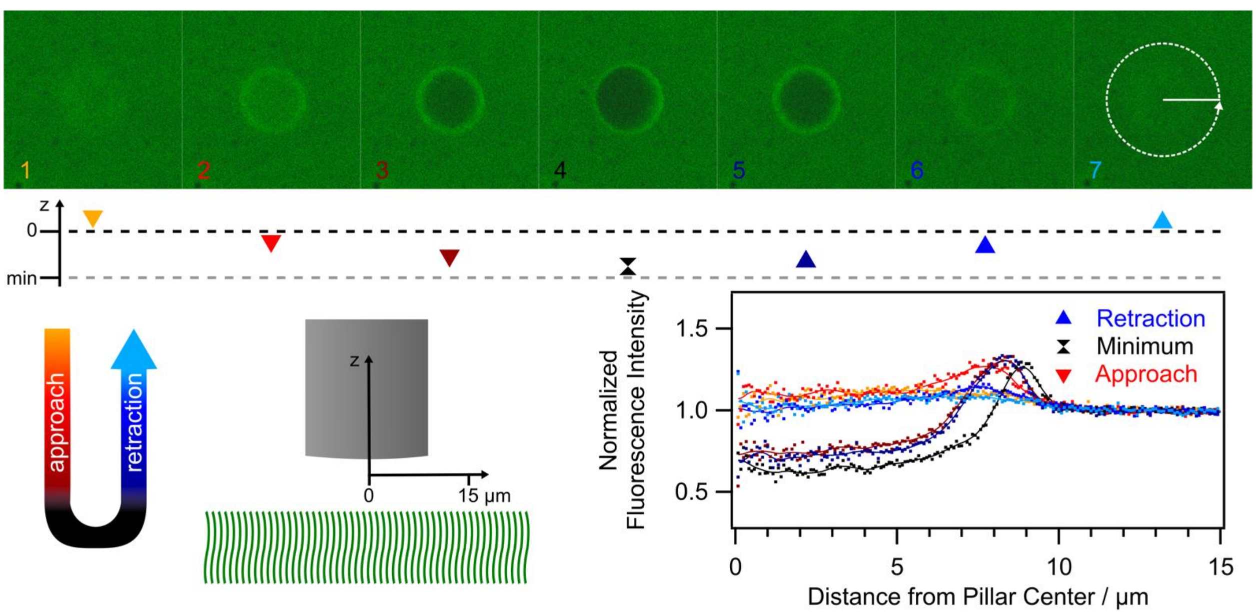

Figure 3. Top: Confocal laser scanning microscopy images of an individual flat punch pillar during approach (images 1-3), at the minimum (image 4), and during retraction (images 5-7). Below, the z-

position is plotted relatively to the minimum position and the position of the first noticeable change of fluorescence. The fluorescence intensity was averaged azimuthally, as implied in image 7 (radius 15 µm), and plotted on the **bottom right**. For normalization, the fluorescence intensity was related to the equilibrium intensity outside of the contact area. Lines were added to guide the eye. In direct comparison, lower intensity could be related to local compression, and higher intensity to local tension, respectively. **Bottom left:** Scheme of the orientation of the depicted quantities. The color code of approach and retraction corresponds to the image numbers, the symbols on the z-scale, and the radial fluorescence intensity profiles.

In Figure 3, CLSM images during stages of approach (images 1-3, reddish colors) and retraction (images 5-7, bluish colors) are shown. At the minimum of the approach-retraction-cycle (Figure 3, image 4), the azimuthally averaged intensity profile is depicted in black. The corresponding z-position of the stepper motor is depicted below the CLSM images. It was scaled relatively to the starting and the minimum position of the stepper motor. The starting position was defined at the motor step before the first noticeable change of fluorescence. The z-position is scaled relatively because the absolute movement does not correspond to the deformation of the mechano-sensitive surface-coating, the overall deformation scenario is more complex: the z-stepper movement is transferred into the deformation of the polymeric surface, the deformation of the pillars, the deformation of the bulged support and the Laplace pressure from the wetting of the micropillar structures[48,49] so that the deformation of the surface or the pillars cannot be quantified precisely. The equilibrium fluorescence outside the contact area is not changed, proving that the responsiveness of the polyelectrolyte brush is not affected by this wetting phenomenon.

Comparing approach and retraction, similar stress distributions were observed at equal z-positions. During approach, compressive stress built up over the whole contact area, apparent from the decreasing fluorescence intensity. The fluorescence quenching ceased during retraction. The radial intensity profiles support this observation (Figure 3, bottom right). The profiles at equal z-positions coincide, besides slight differences between the light red (Figure 3, image 2) and the middle blue intensity profile (Figure 3, image 6). It has to be noted that the bright rim at the edges of the pillar might not be due to local tensile stresses, as it already appeared during approach. It might have been an effect of scattering of the excitation laser at the edges of the flat punch pillar. The locally higher excitation intensity would have resulted in a locally increased fluorescence intensity. Optical reflective microscopy images with dark-field condenser confirm the higher scattering intensity at the edges of flat punches (Figure S3).

The contact formation and detachment of T-shaped micropillars was investivated in analogous experiments (Video S4). The fluorescence response during approach and retraction of T-shaped pillars is presented in Figure 4.

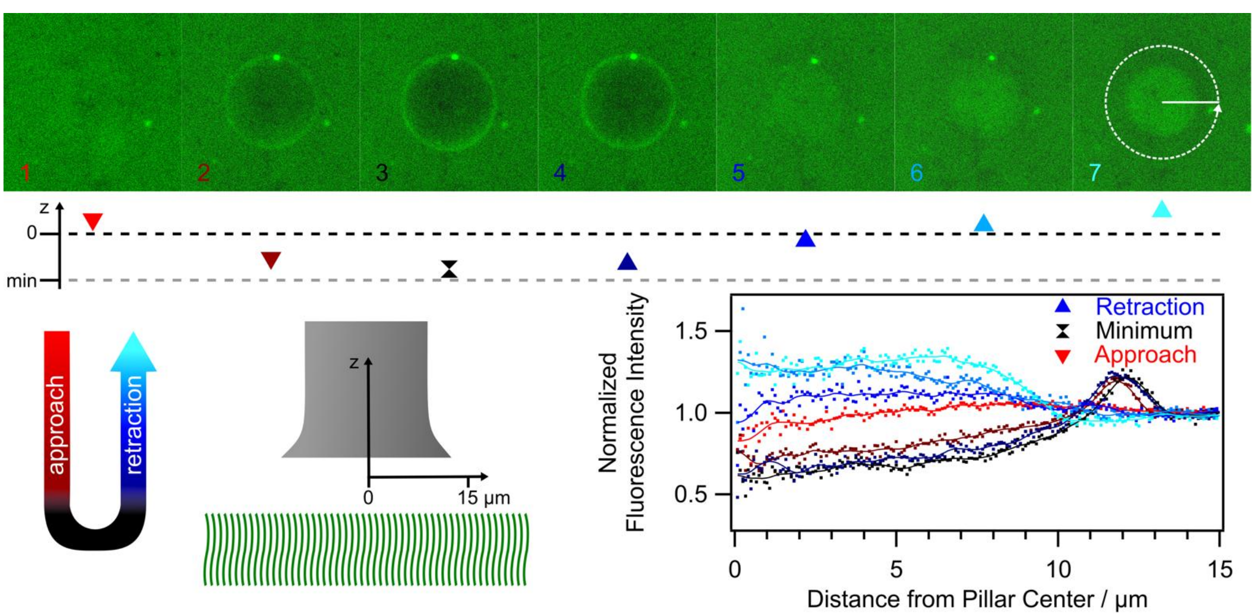

Figure 4. Top: Confocal laser scanning microscopy images of an individual T-shaped pillar during approach (images 1+2), at the minimum (image 3), and during retraction (images 4-7). Below, the z-position is plotted relatively to the minimum position and the position of the first noticeable change of fluorescence. The fluorescence intensity was averaged azimuthally, as implied in image 7, and plotted on the **bottom right**. For normalization, the fluorescence intensity was related to the equilibrium intensity outside of the contact area. Lines were added to guide the eye. In direct comparison, lower intensity could be related to local compression, and higher intensity to local tension, respectively. **Bottom left:** Scheme of the orientation of the depicted quantities. The color code of approach and retraction corresponds to the image numbers, the symbols on the z-scale, and the radial fluorescence intensity profiles.

During approach to minimum (Figure 4, images 1-3, reddish and black), T-shaped pillars do not differ from flat punches qualitatively. Upon retraction (Figure 4, images 4-7, bluish colors), an obvious difference is perceived in the stress distribution.

Retracting below the starting z-position (Figure 4, images 4+5), the quenching diminishes. At the starting z-position (Figure 4, image 6), the fluorescence at the center of the contact area is slightly increased. When the pillars are retracted above the starting z-position (Figure 4, image 7), the fluorescence in the central contact area increases further. In addition, quenching at the edges appears. Before the adhesion breaks up spontaneously, the contact area contracts slightly (Video S4).

In the case of the T-shaped pillars, the increased fluorescence in the center (Figure 4, images 6+7) directly relates to local tensile stresses during detachment. It did not appear during approach. However, in some cases, also fluorescence rims at the edges appeared (Figure 4, images 2-4). We expect them to be caused by the same effect as for the flat punches (Figure S5).

To gather insight into the detachment mechanisms of flat punch and T-shaped pillars, the compressive and tensile areas were deduced from the local fluorescence intensity. For direct comparison, the detachment from the mechano-sensitive surface is sketched schematically for both pillar geometries (Figure 5).

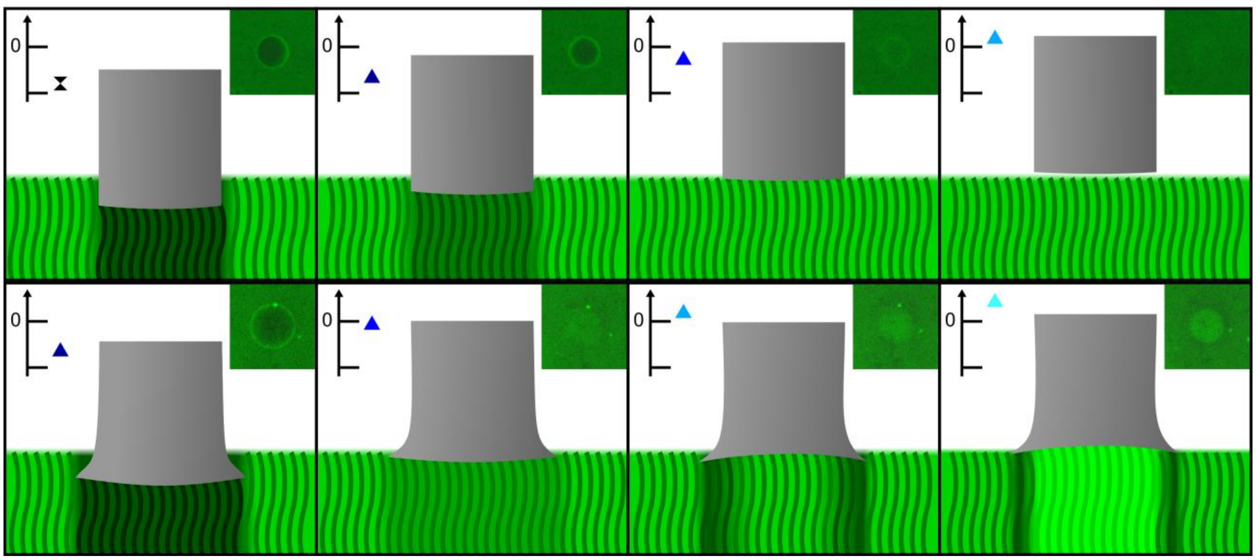

Figure 5. Schematic interpretation of the observed fluorescence response of the mechano-sensitive surface during the retraction of the pillars. From the left to the right, stages of retraction are depicted for flat punch (**top**) and T-shaped pillars (**bottom**). The corresponding inset CLSM images and z-scales are adapted from Figure 3 and Figure 4, respectively. In the depiction, the size of the pillars (approx. 20 µm in height) and the thickness of the mechano-sensitive surface (approx. 150 nm) are not to scale.

The flat punch pillars do not feature an adhesion break-up, but rather a gradual removal from the mechano-sensitive surface. Fading compressive stresses could be assigned to the whole contact area during retraction up to the starting z-position where no mechanical interactions could be recognized anymore.

Several groups calculated the stresses acting during the detachment of flat punches.[35,36,38,40,42] The calculated stress was found to be minimal at the central region of the pillar. Hence, adhesion failure was attributed to stress singularities at the edges allowing detachment cracks to propagate to the center. This is more pronounced for rounded edges.[41]

In our experiments, the flat punch pillars were detached from the mechano-sensitive surface with a fluorescent rim. We attributed this effect to a local fluorescence increase from back-scattering. With the adhesion strength being lower in water,[50] the acting tensile stresses might have been masked by the fluorescence increase from scattering. Nevertheless, the deduced detachment mechanism is in good agreement with the aforementioned literature. Although the scattering and tensile stress contributions to the fluorescence increase at the very edges cannot be distinguished clearly, the compressive stress decreases over the whole contact area from the center towards the edges. In addition, the rupture event is too fast for CLSM. With high-speed video recording, Heepe *et al.* determined the crack propagation speed to the order of magnitude of 1 m/s for flat punch pillars.[32]

During the retraction of the T-shaped pillars, a comparable gradual decrease in compression as for the flat punches could be determined. However, at the original starting position, the annular overhangs seemed to bend towards the mechano-sensitive surface. This was apparent from the acting compressive stresses at the edges of the contact area. When the pillars were further retracted above the original starting point, the behavior during pull-off was recognized. As the tension increased in the center, the compression increased at the edges. Moreover, the contact area was contracted slightly until the pillar was detached spontaneously.

For modeling of T-shapes, their geometry was simplified to be a flat punch with a plate-like cap.[36,40,42] Above a certain plate thickness, the pillars behave like larger flat punches. For thin plates, the stress is minimal at the edges of the plate, but stress peaks appear in the region of the pillar diameter. In between the limiting cases, an almost uniform tension is prominent in the central contact area, decreasing towards the edges.[36] As a consequence, the adhesion failure usually does not originate from the edges, but from the center of the contact area.[32]

Modeling the pull-off of T-shapes with an annular wedge-like geometry, Aksak *et al*. further elucidated the detachment mechanism by varying the wedge angle and the ratio of cap-to-pillar.[39] At steep wedge angles and low cap-to-pillar ratios, singularities appear at the edges, similar to flat punches. By decreasing the wedge angle, the stress at the edges can be reduced.

Although our T-shapes resemble a bell-like shape and might not be compared directly with either of the presented models, we found the main features of the theoretical predictions in the measured stress distributions. Essentially, the tensile stress is concentrated uniformly to the center, and decreases towards the edges.

For our T-shaped pillars, we expect the overhangs to be deformed further during approach and detachment. When retracted, the tensile stress in the central region forces the overhangs to bend down for preserving the contact. This effect intensifies when the T-shaped pillars are pulled off the surface. It can be deduced from the increasing tensile stresses in the center and stronger compression at the edges of the contact area of the pillars. As a result, the contact area contracts permanently until the pillar is detached from the surface. This suction-cup-like bending has been observed before.[22,31,33,51]

Summarizing, our results indicate that the main reason for T-shapes excelling flat punches in adhesion is the suppression of crack formation at the edges of T-shapes. The tensile stresses are concentrated to the center of the contact area, as predicted by theory.

CONCLUSIONS

We determined the contact stress distributions of bioinspired flat punch and T-shaped pillar microstructures with a polymeric mechano-sensitive surface. Utilizing a micro-contact printer, they were approached and retracted normal to the surface. In contact with the surface, increasing compressive stresses over the whole contact area were monitored during approach. Up to the position of contact formation, the compressive stresses decreased again. For flat punch pillars, theory predicts stress singularities at the edges causing cracks to propagate towards the center. However, tensile mechanical interactions could not be determined undoubtedly. Either the acting tensile stresses were below the sensitivity of the polymeric surface, or the adhesion of the flat punches was too low. On the contrary, tensile stress is expected to be minimal at the edges of T-shaped pillars. Indeed, we observed tensile stresses acting in the central contact area during pull-off. Simultaneously, compressive stresses appeared at the edges of the contact area owing to the overhangs bending towards the surface. With the tension increasing in the center, the compression increased at the edges. Additionally, the contact area contracted during pull-off, supporting the depiction of a suction cup-like bending of the overhangs. Consequently, the detachment of the pillars is forced to develop from the center towards the edges. Hence, the adhesion failure originating from the edges is suppressed.

As further perspectives, the presented approach to determine the stress distributions during pull-off might be a powerful tool in further development of biomimetic adhesive microstructures. This technique is valuable in particular for the design of wet adhesion systems. Beyond the specific case of biomimetic adhesion, we believe that mechano-sensitive surfaces as we presented them here can be of interest for clarifying adhesion of soft matter in water, as for instance, hydrogels on polyelectrolyte brushes.[52-54]

EXPERIMENTAL SECTION

Preparation of Biomimetic Micropillar Structures

Silicon wafers (100 orientation) were purchased from Crystec (Berlin, Germany). SU-8 photoresist 2025 and the developer mr-Dev 600 were purchased from Micro Resist Technology (Berlin, Germany). 1H,1H,2H,2H-Perfluorodecyltrichlorosilane (96%) was purchased from Alfa Aesar (Karlsruhe, Germany). PDMS elastomer kits (Sylgard 184) were purchased from Dow Corning (Midland, MI). Masks for lithography were custom-made by ML&C (Jena, Germany).

Thin PDMS precursor films were prepared with a Multicator 411 film applicator (Erichsen, Hemer, Germany). For surface activation, a PlasmaActivate MiniFlecto plasma chamber was used (Plasma Technology, Rottenburg, Germany).

The micro-contact stamps were casted in the custom-made molding stations shipped with the device (µCP-PVM-A from GeSiM, Großerkmannsdorf, Germany).

Detailed information about the preparation of flat punch and T-shaped micropillar structures can be found in our previous publications.[24,29] By photolithographic processing of SU-8, 8x8 mm^2 cubic patterns of micropillars were generated on silicon wafers. The height, the diameter and the spacing of the pillars was 20 µm. To prepare for soft lithography, the silicon masters were perfluorosilanized. A negative of the photolithographic micropillar patterns was cast from polydimethylsiloxane (PDMS) to produce a soft mold. PDMS was mixed in a 10:1 ratio of prepolymer/crosslinker, degassed for 30 minutes, poured onto the SU-8 pattern and cured at 90 ºC for one hour. Before its use as a mold, the negative PDMS replica was perfluorosilanized as well.

Flat punch micropillars were fabricated by molding from the PDMS negative. To produce T-shaped micropillars, flat punches were manually inked in a thin film of PDMS, precured at room temperature for

8-9 hours. Subsequently, the inked pillars were postcured in contact with a perfluorosilanized silicon wafer at 65 ºC for 14 hours. The enlargement of the cap diameter was approximately 35%.

For the micro-contact printing setup, featureless flat stamps were produced for the setup. For their fabrication, unpatterned perfluorosilanized silicon wafers were placed as masters in the molding stations for the micro-contact printing stamps. A gasket between the stamp blank and the unpatterned master defined the height of the stamps. To further constrain the cavity, a cylindrical block was inserted into the stamp blank. PDMS was injected into the cavity of the stamp blank. After curing for 4 hours at 65 ºC, the stamps were removed from the molding stations and demolded from the gasket and the block. By inking the backside of the pillar microstructures with PDMS, they were attached to the stamps, and fixed by curing the connecting layer at 90 ºC for one hour.

Preparation of Mechano-Sensitive Surfaces

For the preparation of the mechano-sensitive surfaces, a polyelectrolyte brush was synthesized in a grafting from-approach. As the surface initiator, 3-(Trimethoxysilylpropyl)-2-bromo-methylpropionate (95 %) was purchased from Gelest (Morrisville, PA, USA). Methacryloyloxyethyltrimethyl ammonium chloride (METAC, 80 wt.% aqueous solution), 2- aminoethyl methacrylate hydrochloride (AEMA, 90 %), triethylamine (99 %), 2,2'-bipyridine (99 %), copper(II)-chloride (99.999 %), copper(I)-bromide (99.999 %), 5(6)-carboxyfluorescein N-hydroxysuccinimide ester, dry toluene (99.8 %), and dimethyl sulfoxide (DMSO, 99.5 %) were purchased from Sigma-Aldrich Co. Round cover slips (Ø 24 mm) were purchased from VWR International GmbH (Germany). Deionized water was purified with a Milli-Q system (Merck Millipore, Darmstadt, Germany).

The mechano-responsive polymer structures were prepared in a surface-initiated controlled radical polymerization, as published elsewhere.[43] Briefly, round cover slips were used as substrates. They were cleaned by sonication and oxygen plasma treatment, directly followed by immersion into a solution of surface-initiator in toluene. After attachment overnight, the surface-initiator was fixed at 150 ºC for 4 hours. Each substrate was placed in a separate Schlenk tube under argon atmosphere. An isopropyl alcohol/water solution [7/2 (v/v)] of the monomers (METAC and AEMA [ratio 10 000:1]), copper(II)-chloride, and bipyridine were dissolved and degassed. Under argon atmosphere, copper(I)-bromide was added to the polymerization solution. It was dispensed among the substrate-loaded Schlenk tubes and left for 4 hours at room temperature under argon atmosphere. Then, the polymerization was quenched with ethanol.

For labeling, the substrates were immersed in 0.1 M hydrogen carbonate solution. Carboxyfluorescein was dissolved in DMSO and added to the immersed substrates. Overnight, the dye covalently bonded to the comonomer AEMA. Excess was removed by subsequent sonication in 1 M sodium chloride solution and water.

Determination of Contact Stress Distributions

The contact formation of the stamps with the structures was controlled with a µCP-PVM-A micro-contact printer from GeSiM (Großerkmannsdorf, Germany). For a plane contact formation, the system is able to bulge the stamp by applying an overpressure (130-140 kPa) to compensate the concavity originating from the preparation. The movement of the stamps towards and away from the surface was performed with a stepper motor.

The micro-contact printer and the mechano-sensitive surfaces were aligned on an Axio Observer Z.1 inverted microscope combined with an LSM710 confocal laser scanning module (Carl Zeiss Microscopy, Jena, Germany) to monitor the fluorescence response during contact. For the measurements, the cover slip with the mechano-sensitive surface was fixed on a glass slide with a droplet of water in between. Before the measurements, the mechano-responsive polyelectrolyte surface coating was wetted with Milli-Q water. After the measurements, the mechano-sensitive surface coating was regenerated by extensive rinsing with Milli-Q water.

For the read-out of the mechano-response, the fluorescein dye was excited with an Ar laser at a wavelength of 488 nm from LASOS (Jena, Germany). Emission was detected at a wavelength interval from 493-685 nm. The pinhole size was fixed to 1 Airy unit (4.4 µm). As objective, an EC Epiplan-Neofluar 20x/NA 0.5 was used (Carl Zeiss Microscopy, Jena, Germany).

The azimuthally averaged intensity profiles were generated with the Radial Profile Plugin (v.2009) in ImageJ 1.50d.

Electron Microscopy

The shape of the micropillars was determined with scanning electron microscopy using a Zeiss Leo Gemini 1530 (Carl Zeiss Microscopy, Jena, Germany) equipped with a field-emission cathode with an operating voltage of 3 kV. Beforehand, the samples were sputtered with a 3 nm Platinum layer.

SUPPORTING INFORMATION

Supporting Information is available online. The following files are available free of charge. Supplemental Data (PDF), Videos of the CLSM images of flat punch and T-shaped pillars on the mechano-sensitive surface (mp4).

AUTHOR INFORMATION

Corresponding Authors

* Aránzazu del Campo, Tel. +49 681 9300 510, aranzazu.delcampo@leibniz-inm.de

* Andreas Fery, Tel. +49 351 4658 225, fery@ipfdd.de

Author Contributions

The manuscript was written through contributions of all authors. All authors have given approval to the final version of the manuscript.

Notes

The authors declare no competing financial interest.

ACKNOWLEDGMENT

The authors thank the Deutsche Forschung Gemeinschaft for financial support within the program SPP1420 “Biomimetic Materials Research: Functionality by Hierarchical Structuring of Materials” (Projects CA 880/1, FE 600/16-3). L.X. thanks the National Natural Science Foundation of China (51503156) for support. A.d.C. thanks the European Union for financial support (ITN BioSmartTrainee 642861). Further, we thank Roland Höller for the SEM images and Sebastian Rauch for support with optical microscopy. J.W.N. acknowledges the support of the Elite Network of Bavaria.

REFERENCES

(1) Arzt, E.; Gorb, S.; Spolenak, R. From Micro to Nano Contacts in Biological Attachment Devices. *PNAS* **2003**, *100* (19), 10603–10606.

(2) Gorb, E. V.; Gorb, S. N. Attachment Ability of the Beetle Chrysolina Fastuosa on Various Plant Surfaces. *Entomologia Experimentalis et Applicata* **2002**, *105* (1), 13–28.

(3) del Campo, A.; Greiner, C.; Álvarez, I.; Arzt, E. Patterned Surfaces with Pillars with Controlled 3D Tip Geometry Mimicking Bioattachment Devices. *Adv. Mater.* **2007**, *19* (15), 1973–1977.

(4) Murphy, M. P.; Kim, S.; Sitti, M. Enhanced Adhesion by Gecko-Inspired Hierarchical Fibrillar Adhesives. *ACS Appl Mater Interfaces* **2009**, *1* (4), 849–855.

(5) Hu, H.; Tian, H.; Li, X.; Shao, J.; Ding, Y.; Liu, H.; An, N. Biomimetic Mushroom-Shaped Microfibers for Dry Adhesives by Electrically Induced Polymer Deformation. *ACS Appl Mater Interfaces* **2014**, *6* (16), 14167–14173.

(6) Afferrante, L.; Carbone, G. Biomimetic Surfaces with Controlled Direction-Dependent Adhesion. *J. R. Soc. Interface* **2012**, *9* (77), 3359–3365.

(7) Wang, Z.; Gu, P.; Wu, X. A Gecko-Inspired Double-Sided Adhesive. *Phys Chem Chem Phys* **2013**, *15* (47), 20764–20770.

(8) Yi, H.; Hwang, I.; Sung, M.; Lee, D.; Kim, J.-H.; Kang, S. M.; Bae, W.-G.; Jeong, H. E. Bio-Inspired Adhesive Systems for Next-Generation Green Manufacturing. *Int. J. of Precis. Eng. and Manuf.-Green Tech.* **2014**, *1* (4), 347–351.

(9) Gorb, S.; Varenberg, M.; Peressadko, A.; Tuma, J. Biomimetic Mushroom-Shaped Fibrillar Adhesive Microstructure. *J. R. Soc. Interface* **2007**, *4* (13), 271–275.

(10) Xue, L.; Kovalev, A.; Eichler-Volf, A.; Steinhart, M.; Gorb, S. N. Humidity-Enhanced Wet Adhesion on Insect-Inspired Fibrillar Adhesive Pads. *Nat Commun* **2015**, *6*, 6621.

(11) Glassmaker, N. J.; Jagota, A.; Hui, C.-Y.; Noderer, W. L.; Chaudhury, M. K. Biologically Inspired Crack Trapping for Enhanced Adhesion. *Proc. Natl. Acad. Sci. U.S.A.* **2007**, *104* (26), 10786–10791.

(12) Paretkar, D.; Kamperman, M.; Martina, D.; Zhao, J.; Creton, C.; Lindner, A.; Jagota, A.; McMeeking, R.; Arzt, E. Preload-Responsive Adhesion: Effects of Aspect Ratio, Tip Shape and Alignment. *J. R. Soc. Interface* **2013**, *10* (83), 20130171.

(13) Bartlett, M. D.; Croll, A. B.; King, D. R.; Paret, B. M.; Irschick, D. J.; Crosby, A. J. Looking Beyond Fibrillar Features to Scale Gecko-Like Adhesion. *Adv. Mater.* **2012**, *24* (8), 1078–1083.

(14) Spolenak, R.; Gorb, S.; Arzt, E. Adhesion Design Maps for Bio-Inspired Attachment Systems. *Acta Biomater* **2005**, *1* (1), 5–13.

(15) Boesel, L. F.; Greiner, C.; Arzt, E.; del Campo, A. Gecko-Inspired Surfaces: a Path to Strong and Reversible Dry Adhesives. *Adv. Mater.* **2010**, *22* (19), 2125–2137.

(16) Ohler, A. Digital Pad Morphology in Torrent-Living Ranid Frogs. *Asiatic Herpetological Research* **1995**, *6*, 85–96.

(17) Federle, W.; Barnes, W. J. P.; Baumgartner, W.; Drechsler, P.; Smith, J. M. Wet but Not Slippery: Boundary Friction in Tree Frog Adhesive Toe Pads. *J. R. Soc. Interface* **2006**, *3* (10), 689–697.

(18) Drotlef, D.-M.; Stepien, L.; Kappl, M.; Barnes, W. J. P.; Butt, H.-J.; del Campo, A. Insights Into the Adhesive Mechanisms of Tree Frogs Using Artificial Mimics. *Adv. Funct. Mater.* **2013**, *23* (9), 1137–1146.

(19) Iturri, J.; Xue, L.; Kappl, M.; García Fernández, L.; Barnes, W. J. P.; Butt, H.-J.; del Campo, A. Torrent Frog-Inspired Adhesives: Attachment to Flooded Surfaces. *Adv. Funct. Mater.* **2015**, *25* (10), 1499–1505.

(20) Autumn, K.; Sitti, M.; Liang, Y. A.; Peattie, A. M.; Hansen, W. R.; Sponberg, S.; Kenny, T. W.; Fearing, R.; Israelachvili, J. N.; Full, R. J. Evidence for Van Der Waals Adhesion in Gecko Setae. *PNAS* **2002**, *99* (19), 12252–12256.

(21) Huber, G.; Gorb, S. N.; Spolenak, R.; Arzt, E. Resolving the Nanoscale Adhesion of Individual Gecko Spatulae by Atomic Force Microscopy. *Biol. Lett.* **2005**, *1* (1), 2–4.

(22) Varenberg, M.; Gorb, S. A Beetle-Inspired Solution for Underwater Adhesion. *J. R. Soc. Interface* **2008**, *5* (20), 383–385.

(23) Greiner, C.; del Campo, A.; Arzt, E. Adhesion of Bioinspired Micropatterned Surfaces: Effects of Pillar Radius, Aspect Ratio, and Preload. *Langmuir* **2007**, *23* (7), 3495–3502.

(24) Xue, L.; Iturri, J.; Kappl, M.; Butt, H.-J.; del Campo, A. Bioinspired Orientation-Dependent Friction. *Langmuir* **2014**, *30* (37), 11175–11182.

(25) Heepe, L.; Gorb, S. N. Biologically Inspired Mushroom-Shaped Adhesive Microstructures. *Annu. Rev. Mater. Res.* **2014**, *44* (1), 173–203.

(26) Aksak, B.; Murphy, M. P.; Sitti, M. Adhesion of Biologically Inspired Vertical and Angled Polymer Microfiber Arrays. *Langmuir* **2007**, *23* (6), 3322–3332.

(27) Purtov, J.; Frensemeier, M.; Kroner, E. Switchable Adhesion in Vacuum Using Bio-Inspired Dry Adhesives. *ACS Appl Mater Interfaces* **2015**, *7* (43), 24127–24135.

(28) Murphy, M. P.; Aksak, B.; Sitti, M. Gecko-Inspired Directional and Controllable Adhesion. *Small* **2009**, *5* (2), 170–175.

(29) del Campo, A.; Greiner, C.; Arzt, E. Contact Shape Controls Adhesion of Bioinspired Fibrillar Surfaces. *Langmuir* **2007**, *23* (20), 10235–10243.

(30) Hossfeld, C. K.; Schneider, A. S.; Arzt, E.; Frick, C. P. Detachment Behavior of Mushroom-Shaped Fibrillar Adhesive Surfaces in Peel Testing. *Langmuir* **2013**, *29* (49), 15394–15404.

(31) Varenberg, M.; Gorb, S. Close-Up of Mushroom-Shaped Fibrillar Adhesive Microstructure: Contact Element Behaviour. *J. R. Soc. Interface* **2008**, *5* (24), 785–789.

(32) Heepe, L.; Kovalev, A. E.; Filippov, A. E.; Gorb, S. N. Adhesion Failure at 180 000 Frames Per Second: Direct Observation of the Detachment Process of a Mushroom-Shaped Adhesive. *Phys. Rev. Lett.* **2013**, *111* (10), 104301.

(33) Heepe, L.; Kovalev, A. E.; Gorb, S. N. Direct Observation of Microcavitation in Underwater Adhesion of Mushroom-Shaped Adhesive Microstructure. *Beilstein Journal of Nanotechnology* **2014**, *5*, 903–909.

(34) Paretkar, D.; Schneider, A. S.; Kroner, E.; Arzt, E. In Situ Observation of Contact Mechanisms in Bioinspired Adhesives at High Magnification. *MRC* **2011**, *1* (01), 53–56.

(35) Creton, C.; Lakrout, H. Micromechanics of Flat-Probe Adhesion Tests of Soft Viscoelastic Polymer Films. *J. Polym. Sci. B Polym. Phys.* **2000**, *38* (7), 965–979.

(36) Carbone, G.; Pierro, E.; Gorb, S. N. Origin of the Superior Adhesive Performance of Mushroom-Shaped Microstructured Surfaces. *Soft Matter* **2011**, *7* (12), 5545–5552.

(37) Carbone, G.; Pierro, E. Sticky Bio-Inspired Micropillars: Finding the Best Shape. *Small* **2012**, *8* (9), 1449–1454.

(38) Aksak, B.; Hui, C.-Y.; Sitti, M. The Effect of Aspect Ratio on Adhesion and Stiffness for Soft Elastic Fibres. *J. R. Soc. Interface* **2011**, *8* (61), 1166–1175.

(39) Aksak, B.; Sahin, K.; Sitti, M. The Optimal Shape of Elastomer Mushroom-Like Fibers for High and Robust Adhesion. *Beilstein Journal of Nanotechnology* **2014**, *5*, 630–638.

(40) Spuskanyuk, A. V.; McMeeking, R. M.; Deshpande, V. S.; Arzt, E. The Effect of Shape on the Adhesion of Fibrillar Surfaces. *Acta Biomater* **2008**, *4* (6), 1669–1676.

(41) Khaderi, S. N.; Fleck, N. A.; Arzt, E.; McMeeking, R. M. Detachment of an Adhered Micropillar From a Dissimilar Substrate. *Journal of the Mechanics and Physics of Solids* **2015**, *75* (C), 159–183.

(42) Balijepalli, R. G.; Begley, M. R.; Fleck, N. A.; McMeeking, R. M.; Arzt, E. Numerical Simulation of the Edge Stress Singularity and the Adhesion Strength for Compliant Mushroom Fibrils Adhered to Rigid Substrates. *International Journal of Solids and Structures* **2016**, *85-86* (C), 160–171.

(43) Bünsow, J.; Erath, J.; Biesheuvel, P. M.; Fery, A.; Huck, W. T. S. Direct Correlation Between Local Pressure and Fluorescence Output in Mechanoresponsive Polyelectrolyte Brushes. *Angew. Chem. Int. Ed.* **2011**, *50* (41), 9629–9632.

(44) Bünsow, J.; Kelby, T. S.; Huck, W. T. S. Polymer Brushes: Routes Toward Mechanosensitive Surfaces. *Acc. Chem. Res.* **2010**, *43* (3), 466–474.

(45) Erath, J.; Schmidt, S.; Fery, A. Characterization of Adhesion Phenomena and Contact of Surfaces by Soft Colloidal Probe AFM. *Soft Matter* **2010**, *6* (7), 1432–1437.

(46) Neubauer, J. W. Structural Properties and Interactions of Mechano-Response Polyelectrolyte Brushes. Master Thesis, University of Bayreuth, Bayreuth, Germany, 2014.

(47) Carbone, G.; Pierro, E. Effect of Interfacial Air Entrapment on the Adhesion of Bio-Inspired Mushroom-Shaped Micro-Pillars. *Soft Matter* **2012**, *8* (30), 7904–7906.

(48) Papadopoulos, P.; Deng, X.; Mammen, L.; Drotlef, D.-M.; Battagliarin, G.; Li, C.; Müllen, K.; Landfester, K.; del Campo, A.; Butt, H.-J.; et al. Wetting on the Microscale: Shape of a Liquid Drop on a Microstructured Surface at Different Length Scales. *Langmuir* **2012**, *28* (22), 8392–8398.

(49) Hensel, R.; Helbig, R.; Aland, S.; Braun, H.-G.; Voigt, A.; Neinhuis, C.; Werner, C. Wetting Resistance at Its Topographical Limit: the Benefit of Mushroom and Serif T Structures. *Langmuir* **2013**, *29* (4), 1100–1112.

(50) Lee, H.; Lee, B. P.; Messersmith, P. B. A Reversible Wet/Dry Adhesive Inspired by Mussels and Geckos. *Nature* **2007**, *448* (7151), 338–341.

(51) Heepe, L.; Varenberg, M.; Itovich, Y.; Gorb, S. N. Suction Component in Adhesion of Mushroom-Shaped Microstructure. *J. R. Soc. Interface* **2011**, *8* (57), 585–589.

(52) La Spina, R.; Tomlinson, M. R.; Ruiz-Pérez, L.; Chiche, A.; Langridge, S.; Geoghegan, M. Controlling Network–Brush Interactions to Achieve Switchable Adhesion. *Angew. Chem. Int. Ed.* **2007**, *46* (34), 6460–6463.

(53) Sudre, G.; Olanier, L.; Tran, Y.; Hourdet, D.; Creton, C. Reversible Adhesion Between a Hydrogel and a Polymer Brush. *Soft Matter* **2012**, *8* (31), 8184–8193.

(54) Yuk, H.; Zhang, T.; Lin, S.; Parada, G. A.; Zhao, X. Tough Bonding of Hydrogels to Diverse Non-Porous Surfaces. *Nat Mater* **2015**, *15* (2), 190–196.

TOC FIGURE

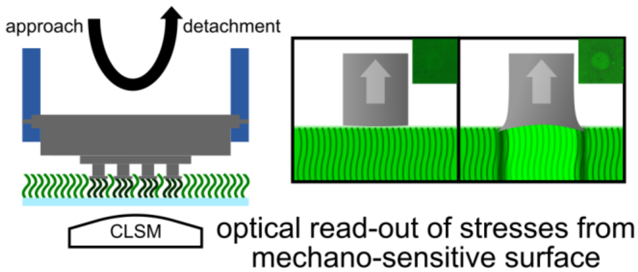
approach
detachment
CLSM
optical read-out of stresses from
mechano-sensitive surface